TEMPERATURE-DEPENDENT RESISTIVITY AND CONDUCTION MECHANISMS IN Co AND F CODOPED NiO THIN FILMS

RESISTIVIDAD Y MECANISMOS DE CONDUCCIÓN DEPENDIENTES DE LA TEMPERATURA EN CAPAS DELGADAS DE NiO CODOPADOS CON Co Y F

Said Benramache†, Ali Arif, Abderrazak Guettaf, Amira Sbaihi, Nadjat Chaouch, Abdelghani Lakel, Okba Belahssen

Laboratoire des Matériaux, des Énergies et de l'Environnement, University of Biskra 07000, Algeria. s.benramache@univ-biskra.dz
† corresponding author

Recibido 1/4/2026; Aceptado 18/6/2026

Co- and F-codoped NiO thin films were successfully deposited on glass substrates using the pneumatic spray deposition method at 420°C. The influence of temperature (T) and dopant concentrations on the electrical and optical properties were investigated. Electrical measurements were carried out in two stages by evaluating the voltage and current over the temperature range of 30–180°C. The temperature affected both voltage and current, with higher T's leading to an enhanced electrical response. The lowest electrical resistivity was achieved for the film doped with 2 % Co and 12 % F. Optical analysis revealed that the films exhibited high transparency in the visible region. Furthermore, the optical band gap increased with increasing Co and F concentrations in all samples. A minimum Urbach energy of 0.342 eV was observed for the film containing 2 % Co and 8 % F, indicating a reduction in localized states within the band tails and an improvement in optical quality.

Se depositaron exitosamente películas delgadas de NiO codopadas con Co y F sobre sustratos de vidrio utilizando el método de deposición por aspersión neumática a 420 °C. Se investigó la influencia de la temperatura (T) y las concentraciones de dopantes en las propiedades eléctricas y ópticas. Las mediciones eléctricas se realizaron en dos etapas, evaluando el voltaje y la corriente en el rango de temperatura de 30–180 °C. La temperatura afectó tanto al voltaje como a la corriente, observándose que temperaturas más altas conducen a una respuesta eléctrica mejorada. La resistividad eléctrica más baja se obtuvo para la película dopada con 2 % de Co y 12 % de F. El análisis óptico reveló que las películas exhibieron una alta transparencia en la región visible. Además, el gap de energía óptica aumentó con el incremento de las concentraciones de Co y F en todas las muestras. Se observó una energía de Urbach mínima de 0.342 eV para la película que contenía 2 % de Co y 8 % de F, lo que indica una reducción en los estados localizados dentro de las colas de banda y una mejora en la calidad óptica.

Keywords: NiO; Thin films (láminas delgadas); Co and F cooping (codopaje con Co y F); TCO; spray pneumatic method (Método del Spray Neumático)

I. INTRODUCTION

Nickel oxide (NiO) is considered an important semiconductor for environmental monitoring due to its ability to detect hazardous gases [1]. It has been employed in a wide range of applications, including gas sensors, fuel-cell electrodes, thermoelectric systems, dye-sensitized solar cells (DSSCs), electrochromic display materials, and catalytic processes [2–8]. For gas-sensing applications, the selection of a suitable material depends on understanding its interaction mechanisms, which are strongly related to its semiconducting electrical behavior and optical transparency. Experimental studies have demonstrated that NiO possesses high optical transparency along with acceptable electrical conductivity under various preparation conditions. Moreover, NiO thin films exhibit a direct optical band gap typically ranging from 3.5 to 4.3 eV [9, 10].

The main objective of this work is to investigate a new material consisting of Co- and F-codoped NiO thin films intended for use as p-type transparent conducting oxides. Regarding the choice of Co and F co-dopants, cobalt (Co) was selected as a transition metal dopant due to its ability to substitute Ni^{2+} sites in NiO and introduce additional *3d* states, which can significantly modify the electronic structure, defect density, and magnetic/electrical properties. Fluorine (F), on the other hand, was chosen as an anion dopant because it can replace oxygen (O^{2-}) sites and act as an effective shallow donor, thereby increasing carrier concentration and improving electrical conductivity. The combined Co and F co-doping strategy was therefore employed to simultaneously tune both cationic and anionic sublattices, aiming to achieve a synergistic improvement in structural, optical, and electrical properties. To the best of our knowledge, NiO thin films simultaneously doped with Co and F have not been previously reported. The advantages of this co-doping approach include enhanced control over defect states, improved tunability of band structure, and simultaneous modulation of conductivity and optical transparency. Previous studies on codoped NiO have mainly focused on other combinations, such as Fe–Li, Li–Cu, and Li–Ti systems.

The selected doping concentrations were maintained within a low levels to prevent secondary phase formation and ensure that the dopants remained below the solubility limit of the NiO lattice [11]. This approach enables the investigation of defect engineering and lattice perturbation effects while minimizing the influence of structural phase transitions [12, 13]. Egbo

et al. [14] reported that effective p-type doping in NiO requires dopants with low formation and ionization energies to enhance solubility and carrier concentration. However, excessive doping can induce compensating donor defects, reducing doping efficiency and p-type conductivity.

Yan et al. [15] investigated the structural and magnetic properties of of $Ni_{0.98}Fe_{0.02}O$ and $Ni_{0.93}Fe_{0.02}Li_{0.05}O$ thin films prepared by pulsed laser deposition. The samples exhibited ferromagnetic behavior at room temperature, and Li codoping was found to significantly enhance the saturation magnetization of $Ni_{0.98}Fe_{0.02}O$. The authors suggested that the dopants occupy substitutional lattice sites. When Li ions are incorporated into NiO, strong hybridization occurs at the Fermi level between the spin-split acceptor band and the Fe *3d* electronic states.

Chen et al. [16] prepared p-type Li–Cu codoped NiO thin films using a chemical solution deposition method and evaluated their optical and electrical performance. The results showed that, for $Li_xCu_{0.1}Ni_{0.9-x}O$ compositions, both optical transmittance and electrical conductivity increased with higher Li concentration (x). In addition, the resistivity of the deposited films decreased significantly, reaching 0.046 $\Omega \cdot$ cm for the $Li_xCu_{0.1}Ni_{0.8}O$ thin film.

Qureshi et al. [17] explored Li- and Ti-codoped NiO nanocomposites for gas-sensing applications at room temperature. Transmission electron microscopy (TEM) analysis revealed particle sizes in the range of 5–40 nm. The sensor exhibited its highest sensitivity toward toluene vapor under room-temperature operating conditions.

In this study, Co- and F-codoped NiO thin films were synthesized using a pneumatic spray deposition technique at 420 °C. The optical and electrical properties were analyzed as a function of dopant concentration, and the electrical behavior was further evaluated over a temperature range of 30–180 °C.

II. EXPERIMENTAL PROCEDURE

For the preparation of Co- and F-codoped NiO films, precursor solutions were obtained by dissolving 0.1 mol.l-1 nickel chloride hexahydrate ($NiCl_2$, $6H_2O$, CAS 7791-20-0) (99.7 % purity) together with cobalt chloride dihydrate ($CoCl_2$, $2H_2O$, CAS 14216-74-1) (99.8 % purity), using Co/Ni ratios of 0.02 and 0.03. Ammonium fluoride (NH_4F, CAS 12125-01-8) (98 % purity) was added as the fluorine source at F/Ni ratios of 0.04, 0.08, and 0.12. The reagents were dissolved in equal volumes of absolute ethanol (99.995 % purity). Three drops of HCl were introduced as a stabilizing agent, and the resulting mixture was stirred for 120 minutes at 50 °C until a clear, transparent solution was obtained.

The five samples of Co- and F codoped NiO precursor solutions were deposited onto heated glass substrates using the pneumatic spray technique. The solution was atomized into fine droplets with an average diameter of approximately 25 μm. Deposition was carried out at a substrate temperature of 420 °C and a solution flow rate of 2 ml $\cdot$ min^{-1}, resulting in uniform thin film formation.

The optical transmittance of the deposited films was measured in the 300 – 700 nm wavelength range using a UV–visible spectrophotometer (LAMBDA 25). The electrical resistance and resistivity of the films were determined using the four-point probe technique with a Keithley 2611B SourceMeter SMU. This instrument provides high-precision current measurements with excellent sensitivity in the picoampere (pA) to nanoampere (nA) range, enabling accurate characterization of highly resistive thin films.

The stabilization periods were applied during the temperature-dependent electrical conductivity measurements, and reproducibility was carefully verified during both heating and cooling cycles. Before each measurement point, the sample was allowed to reach thermal equilibrium at the target temperature. A stabilization time of approximately 2–5 minutes was used after each temperature change to ensure stable temperature and electrical signal. This minimized transient effects and ensured reliable conductivity values. Measurements were then repeated over complete heating and cooling cycles under identical conditions. The resulting conductivity curves showed good agreement between both cycles, with negligible thermal lag, confirming the stability, accuracy, and reproducibility of the measurements. The experimental setup was maintained under controlled laboratory conditions, with precautions taken to minimize electromagnetic interference, mechanical vibrations, and environmental disturbances.

III. RESULTS AND DISCUSSION

III.1. Electrical resistivity Co and F codoped NiO thin films

The electrical properties of Co- and F-codoped NiO thin films were investigated using the four-point probe method over a temperature range of 30–180 °C. Measurements were conducted in two stages: in the first stage, the voltage and current of the films were recorded as the temperature increased from 30 to 180 °C; in the second stage, the same parameters were measured while the temperature decreased from 180 to 30 °C. In order to study the effect of Co and F codoping on the electrical properties of NiO thin films, we made electrical measurements (sheet resistance R_{sh}, resistivity ρ and conductivity σ) as a function of Co and F concentrations. The sheet resistance of the films was calculated using the following relation [18]:

$$R_{sh} = \frac{\pi}{\ln 2} \cdot \frac{V}{I} \tag{1}$$

Here, (I) represents the measured current and (V) the measured voltage. Regarding the conversion from electrical measurements (mV and nA range) to resistivity values (Ω·cm), the calculation of resistivity and conductivity was performed using the following relations [19]:

$$\rho = dR_{sh} \tag{2}$$

$$\rho = \frac{1}{\sigma} \tag{3}$$

where ρ is the resistivity, $d$is the film thickness, R_{sh} is the sheet resistance, and σ is the conductivity.

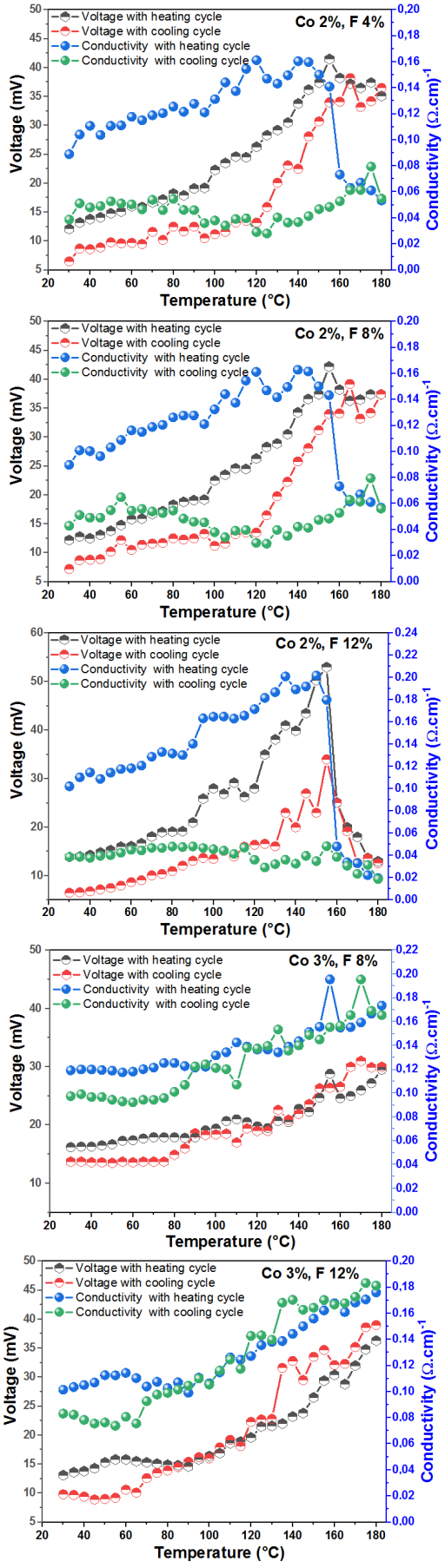

Figure 1. Temperature dependence of voltage and electrical conductivity during heating and cooling cycles for Co and F codoped NiO thin films.

Figure 1 illustrates the variation of voltage with temperature for the Co- and F-codoped NiO films. It can be observed that the voltage increases with increasing temperature during the heating cycle (30 – 180 °C) and decreases with decreasing temperature during the cooling cycle (180 – 30 °C). Moreover, the voltage values measured during the heating cycle were consistently higher than those measured during the cooling cycle. This behavior is likely due to a reduction in the number of mobile charge carriers upon cooling, these results indicate that all deposited Co- and F-codoped NiO thin films are p-type semiconductors [20,21]. The optimum voltage was observed at approximately 160 °C for all deposited films, with the highest value recorded for the film co-doped with 2 % Co and 12 % F.

The electrical conductivity exhibited a different trend during the heating cycle. It initially increased with increasing temperatura from 30 to 160 °C, reaching a maximum value at approximately 150–160 °C. This behavior confirms the semiconducting nature of the codoped NiO films [20], as the supplied thermal energy promotes charge-carrier excitation, thereby enhancing electrical conduction [22, 23]. However, further increasing the temperature beyond this range led to a significant reduction in the conductivity of certain samples. This behavior may be associated with structural rearrangements, increased carrier scattering, desorption of surface species, or the activation of defect states that reduce the concentration of free carriers [20–23].

During the cooling cycle, both voltage and conductivity followed different paths compared to those observed during heating cycle, resulting in a noticeable hysteresis effect. Mohiuddin and Hoa [24] reported that the electrical conductivity exhibits different behaviors during the heating and cooling cycles, leading to the occurrence of electrical hysteresis.

The voltage remained relatively high during cooling before gradually decreasing, while the conductivity did not fully recover its initial values measured during the heating cycle. Such hysteresis behavior is commonly observed in metal oxide semiconductors and may originate from irreversible or slowly reversible processes, including defect redistribution, oxygen adsorption/ desorption, charge-carrier trapping and detrapping of charge carriers, or thermally induced modifications in grain boundary potentials [20–23, 25].

Figure 2 shows the variation of voltage as a function of the measured current for for Co and F codoped NiO thin films, representing their current–voltage (I–V) characteristics. All samples show an increase in voltage with increasing measured current; however, some films exhibits nonlinear I–V behavior and a pronounced hysteresis effect, indicating differences in charge transport mechanisms between the heating and cooling processes, these results indicate that all deposited Co- and F-codoped NiO thin films are p-type semiconductors [26, 27]. The NiO thin film codoped with 2 % Co and 12 % F exhibited improved absorber-layer quality and enhanced

open-circuit voltage, reaching a maximum value of 53 mV at 155 °C.

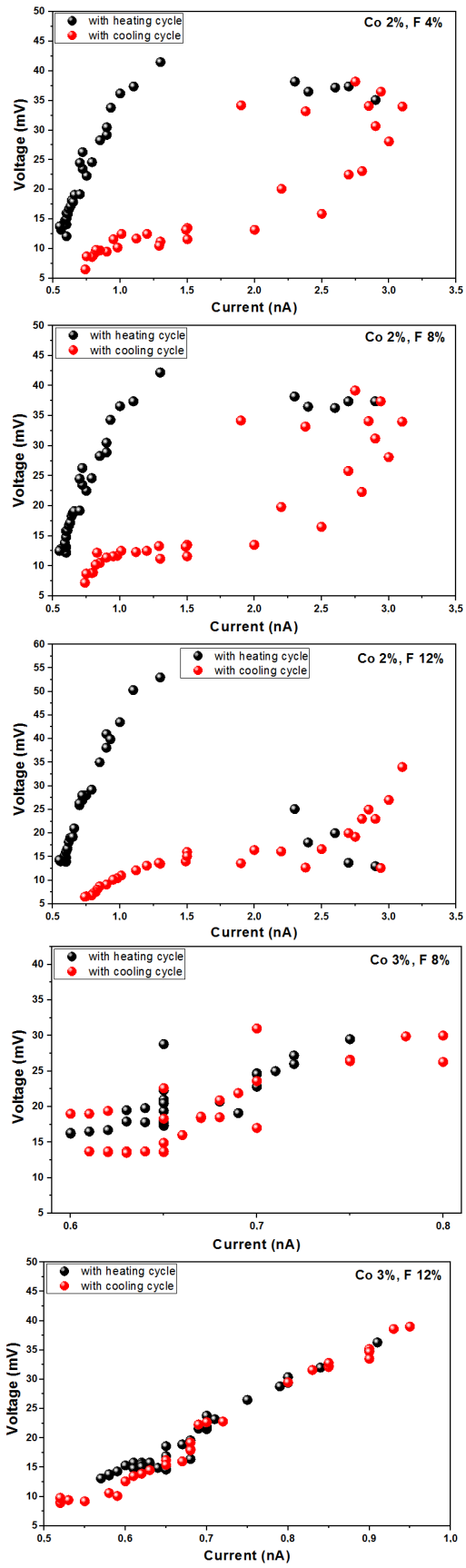

Figure 2. Current–voltage (I–V) characteristics of the Co- and F-codoped NiO thin films measured during the heating and cooling cycles.

Different current ranges were used in Figure 2 to obtain accurate I–V characteristics for each sample, as resistance varies with composition. Co and F codoping changes carrier concentration, defect density, and conductivity of NiO films. Thus, some samples show high resistance and low current, while others exhibit higher conductivity [28]. A single fixed range would reduce resolution or cause saturation. Therefore, the measurement range was adjusted for each sample to keep signals within the instrument's optimal sensitivity, ensuring reliable and precise results.

Figure 3 shows the variation of electrical conductivity of Co and F codoped NiO thin films as a function of (a) heating cycle (b) cooling cycle. During the heating cycle (Figure 3a), all samples show a decrease in electrical resistivity with increasing temperature, indicating a negative temperature coefficient of resistance characteristic of semiconducting behavior. Similar observations have been reported in the literature [29, 30]. The observed behavior is indicative of thermally activated charge transport, whereby elevated temperatures promote charge-carrier mobility and increase the concentration of thermally excited carriers. Significant variations in resistivity are evident among the investigated compositions. Notably, the 2 % Co–12 % F co-doped films exhibit the lowest resistivity values, suggesting that increased co-doping concentrations enhance electrical conduction. This improvement can be associated with the generation of additional electrically active defects (e.g., oxygen vacancies) and enhanced carrier activation, both of which contribute to an increase in free-carrier density and charge-transport efficiency.

During the cooling cycle (Figure 3b), the resistivity does not fully return to its initial values, Indeed, the cooling resistivity is higher than the heating resistivity, resulting in a pronounced thermal hysteresis between the heating and cooling curves. Similar observations have been reported in the literature [20, 21,31]. This behavior suggests the occurrence of irreversible or partially reversible changes during thermal cycling, such as defect reconfiguration, charge-carrier trapping/ detrapping, or the formation of metastable states. The incorporation of Co and F dopants may contribute to these effects by modifying the defect structure and carrier dynamics.

The increase in resistivity during cooling indicates a reduction in the concentration or mobility of thermally activated holes, which are the majority charge carriers in p-type NiO [20, 21], further emphasizing the influence of defect-related mechanisms on the electrical behavior of the films.

The decrease in resistivity with increasing temperature confirms the semiconducting behavior of the Co- and F-codoped NiO films. This behavior is associated with the thermal activation of holes, which are the majority charge carriers in p-type NiO and originate mainly from nickel vacancies and related acceptor defects. Similar observations have been reported in the literature [20–24]. However, the results confirm that Co–F co-doping strongly influences the electrical transport properties of NiO thin films, and the observed hysteresis highlights the role of defect chemistry and thermal activation processes in controlling conductivity.

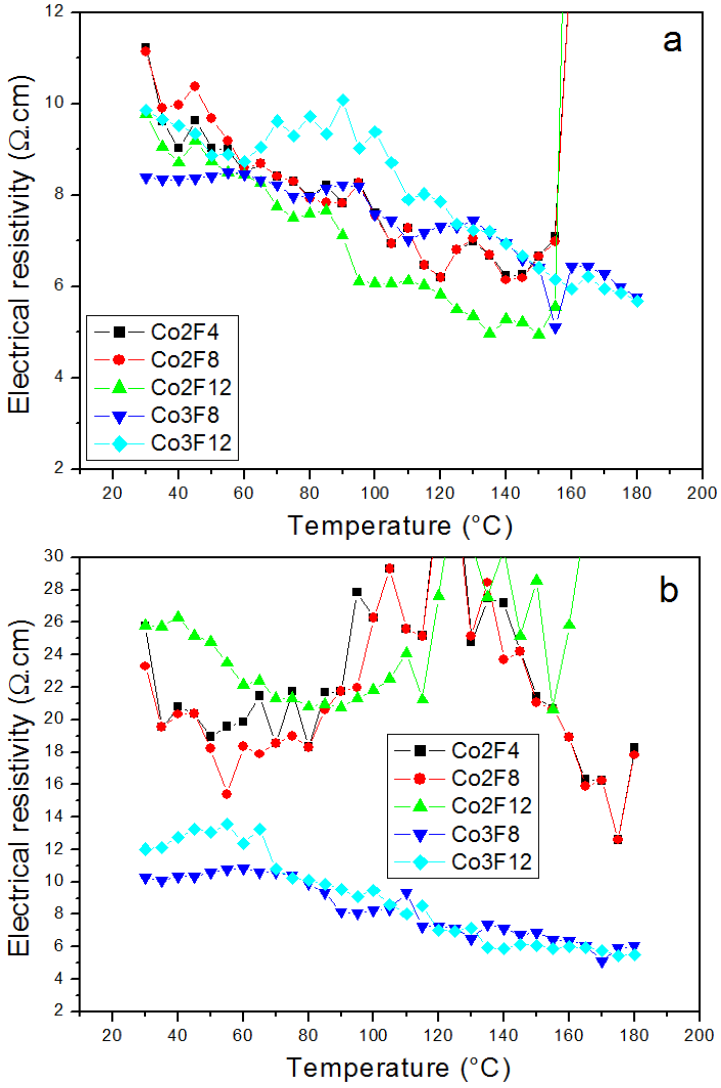

Figure 3. Enter CaptionVariation of electrical conductivity of Co and F codoped NiO thin films as a function of (a): heating cycle (b): cooling cycle.

III.2. Optical property of Co and F codoped NiO thin films

The optical transmittance spectra of Co- and F-codoped NiO thin films at various dopant concentrations are shown in Figure 4, measured over the wavelength range of 300–700 nm. The films exhibited their highest transmittance in the visible region, ranging from 30 % to 65 %. Notably, the film codoped with 3 % Co and 12 % F demonstrated superior transparency, which can be attributed to the substitutional incorporation of Co into the Ni lattice [32]. Furthermore, the enhanced transparency of this film is also associated with the higher F doping concentration, highlighting the combined effect of Co and F codoping on optical performance.

Figure 5 illustrates the absorbance spectra of Co and F codoped NiO thin films in the wavelength range of 300–700 nm. All samples exhibit strong absorption in the UV region followed by a gradual decrease toward the visible region. The film containing 2 % Co and 4 % F shows the highest absorbance, while increasing the fluorine concentration results in a progressive reduction in absorbance. A similar trend is observed for films doped with 3 % Co, with the 3 % Co–12 % F sample exhibiting the lowest absorbance. This behavior suggests that increasing Co and F concentrations enhances the optical transparency of the films and may be associated with modifications in the electronic structure and defect density of the NiO matrix [30,31].

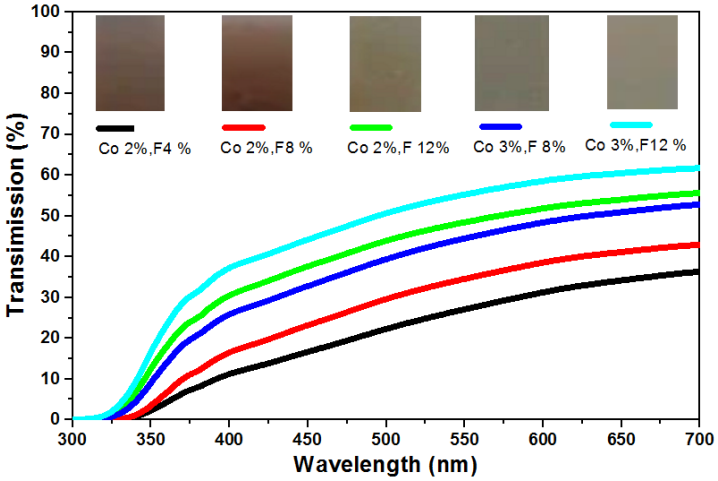

Figure 4. Transmission spectra of Co and F codoped NiO thin films as a function of Co and F concentrations.

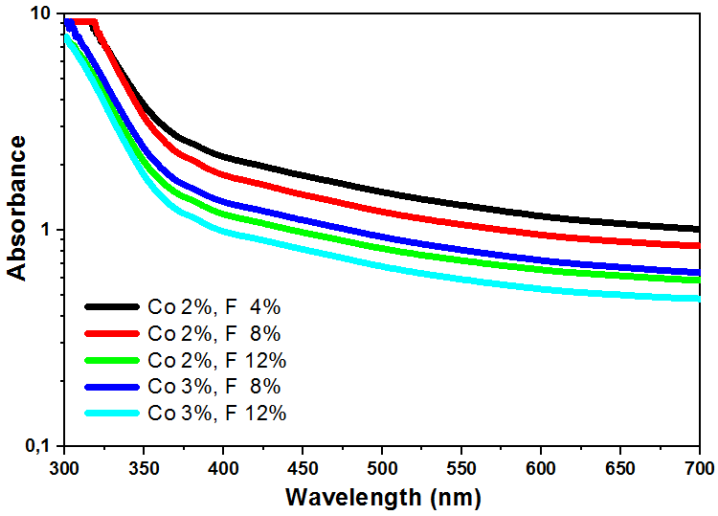

Figure 5. Absorbance spectra of Co and F codoped NiO thin films as a function of Co and F concentrations.

Assuming direct electronic transitions between the valence band and the conduction band, the optical band gap (E_g) of the Co- and F-codoped NiO thin films was determined. The band gap was estimated using Tauc plot method [33], which was constructed from the optical transmittance spectra using the following relations [33,34]:

$$A = \alpha d = -\ln T \quad (4)$$

$$(\alpha h\nu) = B(h\nu - E_g)^n \quad (5)$$

In the above relation, A represents the absorbance, d is the film thickness of prepared thin films; T is the measured transmittance; α denotes the absorption coefficient; B is a constant, $h\nu$ is the photon energy, especially in NiO, $n = 1/2$ for the direct band gap [35] and the band gap energy of Co and F codoped NiO thin films. The optical band gap E was obtained by extrapolating the linear portion of the plot $(Ah\nu)^2$ versus $(h\nu)$ to 0 [36], as illustrated in Figure 6(a).

The use of absorbance instead of the absorption coefficient in Equations (3) and (4) is mainly justified by the experimental constraints and the direct proportionality between both quantities for thin films of known thickness. In thin-film optical measurements, the absorption coefficient α is commonly derived from absorbance A using the relation [37]:

$$\alpha = 2.303 \cdot \frac{A}{d} \tag{6}$$

Since the film thickness is known and uniform within experimental uncertainty, absorbance can be directly used as a proportional representation of absorption coefficient without affecting the qualitative interpretation of the optical transitions.

The assumption of allowed direct transitions in Tauc analysis is supported by both previous studies and the experimental results of this work [35]. Literature reports indicate that NiO thin films, whether doped or undoped, often exhibit direct optical transitions in the high-energy absorption region, particularly in nanostructured or thin-film forms. Therefore, the direct transition model is commonly used to estimate the optical band gap of NiO-based materials. In this study, the Tauc plots $(Ah\nu)^2$ versus $(h\nu)$ show a clear linear region over a wide photon-energy range, confirming an allowed direct transition. The indirect model does not show comparable linearity, supporting this choice.

The optical transmission data were also employed to evaluate the Urbach energy (E_u) of Co and F codoped NiO thin films using the following relation [37,38]:

$$\alpha = \alpha_0 \exp\left(\frac{h\nu}{E_u}\right) \tag{7}$$

In this expression, α_0 is a constant and E_u represents the Urbach energy. The Urbach energy was determined from the slope of the linear region of the $(\ln A)$ versus photon energy $(h\nu)$ plot [39], as illustrated in Figure 6(b). The logarithm used for Urbach energy determination is the natural logarithm *ln* rather than *log*. This correction may slightly influence the visualization and slope of the linear fitting near the absorption edge, but it does not significantly change the overall trend of the results. The estimated uncertainty in the Urbach energy values is about ±0.005 eV, which is typical for optical measurements and fitting methods. Therefore, small differences between close values should be interpreted cautiously.

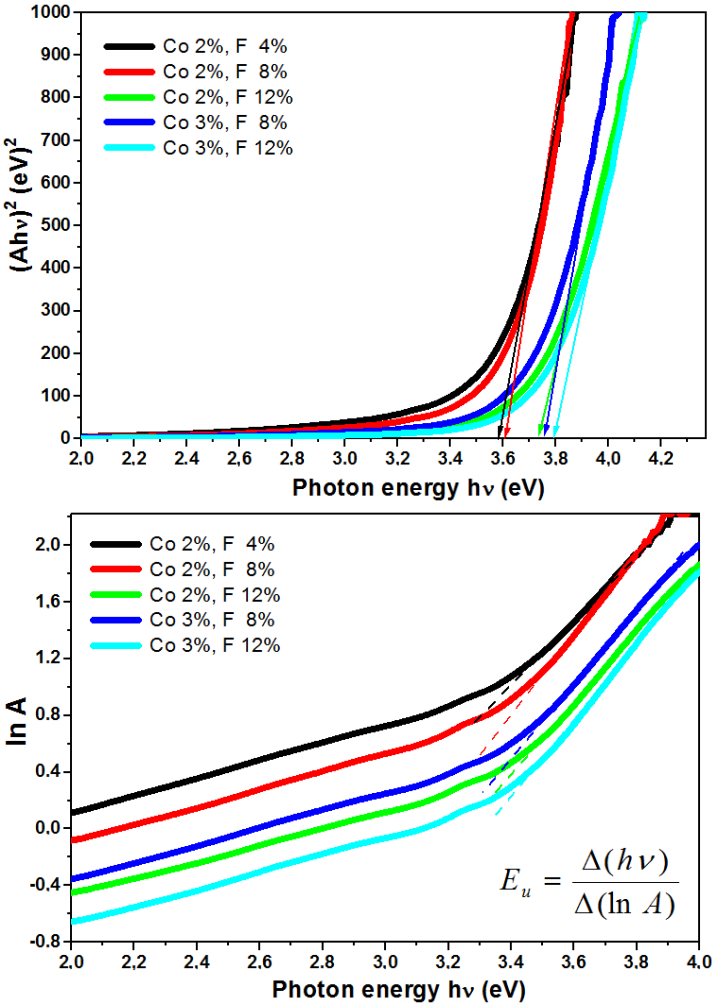

Figure 6. (a): The plot of versus () to determinate of optical band gap energy in NiO thin films as a function of Co and F concentrations and (b): The drawn of $(\ln A)$ versus $(h\nu)$ to determinate of Urbach energy in NiO thin films as a function of Co and F concentrations.

Figure 7 presents the variations of the optical band gap (E_g) and Urbach energy (E_u) for Co- and F-codoped NiO thin films at different dopant concentrations. For a constant Co content, the optical band gap increased with increasing F concentration from 4 % to 12 % and from 8 % to 12 %. This behavior can be attributed to the substitution of F for oxygen rather than nickel, which minimally perturbs the conduction band compared to metal dopants that replace Ni. Consequently, the many-body effects in the conduction band are reduced, even though the addition of F anions raises the Fermi level by filling previously unoccupied conduction band states in the most heavily codoped samples (2 % Co and 12 % F or 3 % Co and 12 % F) [40] (see Table 1). The observed band gap variation is attributed to the combined effect of Co and F codoping, which modifies the electronic structure, carrier concentration, and defect states of the NiO matrix. Dopant incorporation introduces localized energy levels and modifies band tail states, leading to an increase in the optical band gap without forming a new phase, confirming that only the intrinsic NiO transition is observed. The particular behavior observed for the 2 %Co-8 %F sample is not considered an artifact. It may result from an optimal balance between dopant incorporation,

defect density, crystallinity, and carrier concentration, which can strongly influence the optical transition behavior and absorption edge position.

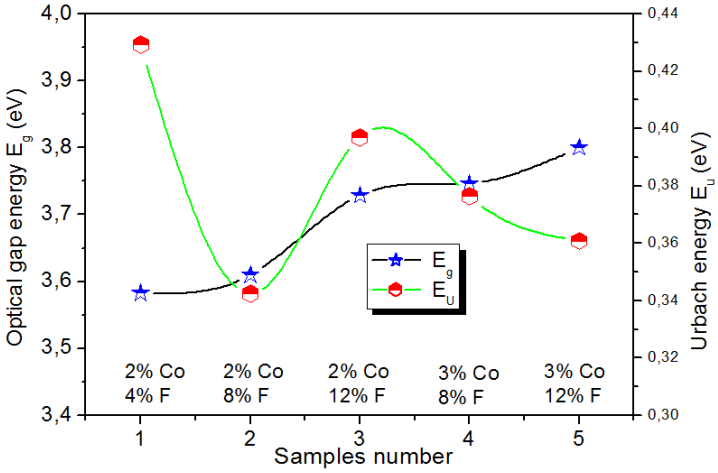

Figure 7. Variation of optical gap energy and Urbach energy of Co and F codoped NiO thin films as a function of Co and F concentrations.

Table 1. Variation of the optical band gap energy E_g and Urbach energy E_u of Co and F codoped NiO thin films.

Co content (%)	F content (%)	E_g (eV) ± 0.005	ΔE_g (eV) ± 0.005	E_u (eV) ± 0.008	ΔE_u (eV) ± 0.008
2	4	3.58	-	0.429	-
2	8	3.61	0.03	0.342	0.087
2	12	3.73	0.12	0.397	0.055
3	8	3.75	0.14	0.376	0.034
3	12	3.80	0.05	0.361	0.015

When the F content is held constant, the band gap also increases with higher Co concentration, e.g., from 2 % Co and 8 % F to 3 % Co and 8 % F, or from 2 % Co and 12 % F to 3 % Co and 12 % F. This effect is attributed to active electronic transitions involving Co^{2+} *3d* levels and the strong sp–d exchange interaction between itinerant sp orbitals of NiO and the localized d orbitals of Co. As a result, the valence band (E_V) narrows downward and the conduction band (E_C) shifts upward, effectively broadening the optical band gap [19].

The minimum Urbach energies of the deposited films were 0.342 eV and 0.361 eV for the 2 % Co–8 % F and 3 % Co–12 % F films, respectively. The decrease in Urbach energy with increasing Co and F concentrations is associated with the widening of the optical band gap, which narrows (E_V) and (E_C) while lowering (E_V) and raising (E_C), thereby reducing the density of localized states in the band tails. The variation of the optical band gap is a key property for advanced materials, particularly for applications in visible-light gas sensing based on metal oxide nanostructures. Figure 8 presents the experimental data and linear fit showing the dependence of the optical band gap on Urbach energy. The broadening of the optical band gap in Co- and F-codoped NiO thin films is attributed to the shifting of the conduction band (E_C) upward and the valence band (E_V) downward, which reduces the overlap and effectively increases the energy separation between the bands.

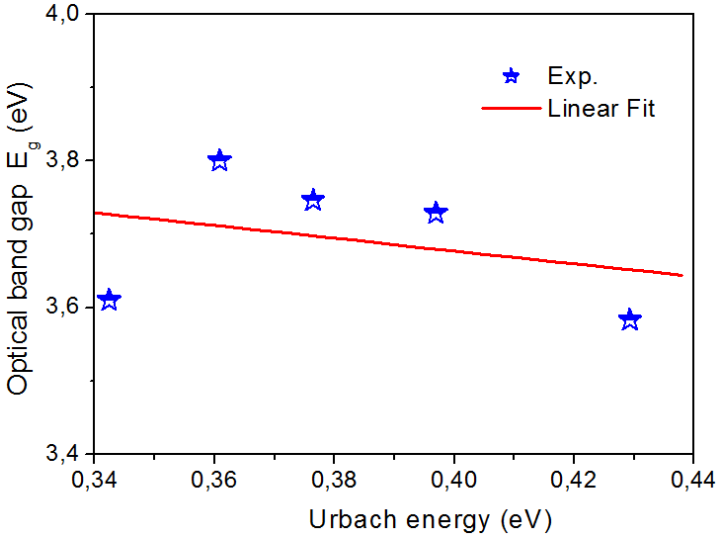

Figure 8. Correlation between optical band gap and Urbach energy of Co and F codoped NiO thin films.

IV. CONCLUSIONS

In this work, Co and F codoped NiO thin films, where Co/Ni = 0.02 and 0.03, F/Ni = 0.04, 0.08 and 0.12, were effectively deposited on glass substrates by spray pneumatic approach utilizing nickel chloride hexahydrate, cobalt chloride dihydrate, and ammonium fluoride. The effects of Co and F co-doping on the electrical and optical characteristics of NiO thin films were examined. The electrical properties of Co and F codoped NiO thin films were investigated at different temperatures, which was based on the calculate the voltage and current of the thin films with increase, from 30 to 180 °C and with reduction, from 180 to 30 °C. We have found that the temperature was affected on the electrical properties; the optimum values of voltage were obtained with increase of temperature. The minimum electrical resistivity of the Co and F co-doping NiO films was located at 2 %Co and 12 %F. The transmission spectra show that the Co and F codoped NiO thin films have the best optical transparent in the visible region. The band gap energy was increased with increasing the Co and F contents in all deposited samples. The minimum Urbach energy was reached at 2 %Co and 8 %F, it is 0.342 eV.

REFERENCES

[1] V. Verma and M. Katiyar, Thin Solid Films **527**, 369 (2013).

[2] S. C. Chen, T. Y. Kuo, Y. C. Lin, and H. C. Lin, Thin Solid Films **519**, 4944 (2011).

[3] R. Sharma, A. D. Acharya, S. B. Shrivastava, M. M. Patidar, M. Gangrade, T. Shripathi, and V. Ganesan, Optik **127**, 4661 (2016).

[4] A. Lakel and S. Benramache, J. Power Technol. **104**, 201 (2024).

[5] A. Lakel, S. Lakel, S. Benramache, and O. Belahssen, J. Chem. Res. **46**, 17475198211066535 (2022).

[6] D. Dini, Y. Halpin, J. G. Vos, and E. A. Gibson, Coord. Chem. Rev. **304–305**, 179 (2015).
[7] G. F. Cai, C. D. Gu, J. Zhang, P. C. Liu, X. L. Wang, Y. H. You, and J. P. Tu, Electrochim. Acta **87**, 341 (2013).
[8] A. C. Nwanya, S. U. Offiah, I. C. Amaechi, S. Agbo, S. C. Ezugwu, B. T. Sone, R. U. Osuji, M. Maaza, and F. I. Ezema, Electrochim. Acta **171**, 128 (2015).
[9] R. Romero, F. Martin, J. R. Ramos-Barrado, and D. Leinen, Thin Solid Films **518**, 4499 (2010).
[10] T. Chtouki, L. Soumahoro, B. Kulyk, H. Bougharraf, B. Kabouchi, H. Erguig, and B. Sahraoui, Optik **128**, 8 (2017).
[11] J. Lennox, R. Pepper, W. Martens, V. Gray, J. Alarco, J. MacLeod, and S. Couperthwaite, Ceram. Int. **52**, 18024 (2026).
[12] C. Mrabet, M. Ben Amor, A. Boukhachem, M. Amlouk, and T. Manoubi, Ceram. Int. **42**, 5963 (2016).
[13] R. S. Kate, S. C. Bulakhe, and R. J. Deokate, Opt. Quantum Electron. **51**, 319 (2019).
[14] K. O. Egbo, C. E. Ekuma, C. P. Liu, and K. M. Yu, Phys. Rev. Mater. **4**, 104603 (2020).
[15] W. Yan, W. Weng, G. Zhang, Z. Sun, Q. Liu, Z. Pan, Y. Guo, P. Xu, S. Wei, Y. Zhang, and S. Yan, Appl. Phys. Lett. **92**, 052508 (2008).
[16] X. Chen, L. Zhao, and Q. Niu, J. Electron. Mater. **41**, 382 (2012).
[17] A. Qureshi, A. Mergen, and A. Altindal, Sens. Actuators B **135**, 537 (2009).
[18] Y. Aoun, M. Marrakchi, S. Benramache, B. Benhaoua, S. Lakel, and A. Cheraf, Mater. Res. **21**, e20170681 (2018).
[19] S. Benramache and B. Benhaoua, Superlatt. Microstruct. **52**, 807 (2012).
[20] I. Hotovy, J. Huran, P. Siciliano, S. Capone, L. Spiess, and V. Rehacek, Sens. Actuators B **78**, 126 (2001).
[21] M. Ben Amor, A. Boukhachem, K. Boubaker, and M. Amlouk, Mater. Sci. Semicond. Process. **27**, 994 (2014).
[22] R. Merienne, J. Lynn, E. McSweeney, and S. M. O'Shaughnessy, Appl. Energy **237**, 671 (2019).
[23] M. Ferrara, H. C. Neitzert, M. Sarno, G. Gorrasi, D. Sannino, V. Vittoria, and P. Ciambelli, Physica E **37**, 66 (2007).
[24] M. Mohiuddin and S. V. Hoa, Compos. Sci. Technol. **72**, 21 (2011).
[25] H. L. Chen, Y. M. Lu, and W. S. Hwang, Surf. Coat. Technol. **198**, 138 (2005).
[26] L. Dejam, J. Sabbaghzadeh, A. Ghaderi, et al., Sci. Rep. **13**, 6518 (2023).
[27] M. Obaida, A. M. Fathi, I. Moussa, and H. H. Afify, J. Mater. Res. **37**, 2282 (2022).
[28] I. L. P. Raj, S. Valanarasu, R. S. R. Isaac, M. Ramudu, Y. Bitla, V. Ganesh, and I. S. Yahia, Optik **254**, 168634 (2022).
[29] A. Hakim, J. Hossain, and K. A. Khan, Renew. Energy **34**, 2625 (2009).
[30] S. Moghe, A. D. Acharya, R. Panda, S. B. Shrivastava, M. Gangrade, T. Shripathi, and V. Ganesan, Renew. Energy **46**, 43 (2012).
[31] P. S. Patil and L. D. Kadam, Appl. Surf. Sci. **199**, 211 (2002).
[32] R. Djarallah, B. Benhaoua, and S. Benramache, Acad. J. Manuf. Eng. **24**, 170 (2026).
[33] J. Tauc, R. Grigorovici, and A. Vancu, Phys. Status Solidi B **15**, 627 (1966).
[34] M. Terlemezoglu, O. Surucu, M. Isik, et al., Appl. Phys. A **128**, 50 (2022).
[35] K. Haunsbhavi, D. Alagarasan, N. J. Shivaramu, et al., J. Electron. Mater. **51**, 6356 (2022).
[36] M. Sh. Abdel-wahab, H. K. El Emam, and W. M. A. El Rouby, J. Mater. Sci.: Mater. Electron. **34**, 1637 (2023).
[37] S. Benramache and B. Benhaoua, Superlatt. Microstruct. **52**, 1062 (2012).
[38] R. Sharma, A. D. Acharya, S. B. Shrivastava, T. Shripathi, and V. Ganesan, Optik **125**, 6751 (2014).
[39] K. Sajilal and A. M. E. Raj, Optik **127**, 1442 (2016).
[40] Y. J. Choi, K. M. Kang, and H. H. Park, Sol. Energy Mater. Sol. Cells **132**, 403 (2015).